First-Principles Study of the Role of Cu in Improving the Coercivity of Nd-Fe-B Permanent Magnets

Y. Tatetsu,[1,*] S. Tsuneyuki,[1,2] and Y. Gohda[1,3,4,†]

[1]*Department of Physics, The University of Tokyo, Tokyo 113-0033, Japan*
[2]*Institute for Solid State Physics, The University of Tokyo, Kashiwa 277-8581, Japan*
[3]*Department of Materials Science and Engineering, Tokyo Institute of Technology, Yokohama 226-8502, Japan*
[4]*ESICMM, RCMSM, National Institute for Materials Science, Tsukuba 305-0047, Japan*

(Received 19 July 2016; revised manuscript received 25 October 2016; published 30 December 2016)

We study the magnetic and electronic properties of Cu-doped $Nd_2Fe_{14}B/NdO_x$ systems with first-principles calculations in order to understand the roles of Cu in improving the coercivity of Nd-Fe-B permanent magnets. By analyzing the formation energies of several model systems, we find that Cu prefers to be at the interface. We conclude that the Cu addition to Nd-Fe-B magnets is a practical way of not only increasing the anisotropy of Nd atoms at the interface but also of lessening the magnetic coupling between the Nd and Fe atoms. Particularly, substituting Fe at the interface of the main phase with Cu works effectively in terms of improving the magnetic anisotropy in Nd atoms. This may explain the coercivity improvements reported recently.

DOI: 10.1103/PhysRevApplied.6.064029

I. INTRODUCTION

Strong magnets are demanded not only for the development of technologies but also for energy saving. Among permanent magnets, Nd-Fe-B magnets are known as the strongest permanent magnets with a high-energy product $(BH)_{max}$ and are widely used in various kinds of applications, for example, high-performance computers, hybrid vehicles, and wind turbines, as well as premium-efficiency motors [1–6]. However, the thermal stability of Nd-Fe-B magnets, especially their coercivity at high temperatures, is a well-known issue, and the mechanism of this low coercivity is an unsolved problem. Recent experimental studies on the microstructures of Nd-Fe-B magnets show that controlling the structural and magnetic properties around the interfaces between main phases and subphases is important for improving the coercivity [7,8]. Wettability around the grain boundaries in Nd-Fe-B magnets is improved by the Nd-Cu grain-boundary diffusion process. In addition, several experimental annealing processes have succeeded in improving the coercivity, which indicates the importance of Cu around the interface [9–19].

Considering these experimental results, the existence of Cu around the interface can be expected to influence the coercivity improvement directly. As reported in several studies [9,11,12,18,19], Cu is thought to be located around the main-phase ($Nd_2Fe_{14}B$) grains. The total amount of Cu atoms is quite small, about 2 at. %. However, the roles of Cu in Nd-Fe-B magnets are still unclear since it is difficult to identify the exact position of the Cu atoms by experiment. Hence, first-principles calculations are an alternative and powerful tool for finding where Cu prefers to be around the interfaces in Nd-Fe-B magnets.

In the present study, we simulate Cu-doped $Nd_2Fe_{14}B/NdO_x$ systems as the first step toward understanding the role of Cu in the coercivity improvement and the magnetic and electronic structures around the interfaces. These systems are discovered around triple junctions in annealed Nd-Fe-B magnets [10,11,20,21]. We study how the magnetic anisotropy in Nd is affected by Cu because this is directly related to the coercivity. We find that Fe at the interface can be replaced by Cu due to having a lower formation energy than the non-Cu-doped system, and this replacement improves the magnetic anisotropy of Nd atoms at the interface. In particular, the anisotropy improvement in Nd near Cu is about 40%. This is one of the reasons for the coercivity improvement.

II. COMPUTATIONAL METHOD

We calculate the formation energies and the magnetic anisotropy of Cu-doped $Nd_2Fe_{14}B/NdO_x$ model systems by using the computational code OpenMX [22], which is based on optimized pseudopotentials and pseudo-atomic-orbital basis functions within density-functional theory (DFT). As basis sets, $s2p2$ configurations are adopted for B and O atoms and $s2p2d2$ for Nd, Fe, and Cu atoms with cutoff radii of 7.0, 7.0, 8.0, 6.0, and 6.0 a.u., respectively. Semicore orbitals of $3s$ and $3p$ in Fe and Cu as well as $5s$ and $5p$ in Nd are treated as valence electrons. In order to reduce computational costs as much as possible, we use an open-core pseudopotential for Nd

*tatetsu@cms.phys.s.u-tokyo.ac.jp
†gohda.y.ab@m.titech.ac.jp

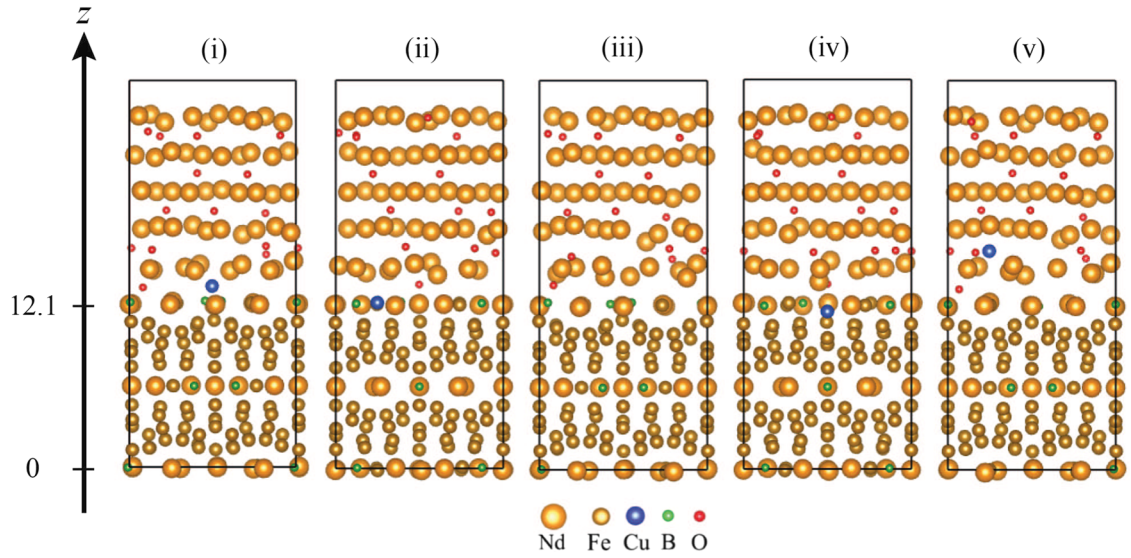

FIG. 1. The interface model structures (i) to (v) of Cu-doped $Nd_2Fe_{14}B/Nd_4O$ systems.

atoms in which well-localized $4f$ electrons are treated as spin-polarized core electrons. The generalized-gradient approximation is used as the Perdew-Burke-Ernzerhof exchange-correlation functional [23]. According to *ab initio* studies of the stable oxygen positions in NdO_x, when $x = 0.25$, oxygen prefers tetrahedral sites to octahedral sites [24], which is consistent with experiments that examined the crystal structure around the interface in Nd-Fe-B sintered magnets [20,21]. Therefore, metallic Nd_4O, in which Nd atoms construct a fcc sublattice and oxygen atoms partially occupy the tetrahedral sites randomly, is adopted as a subphase structure in our model systems. The lattice constants are set to $a = b = 8.75$ Å and $c = 12.1$ Å for $Nd_2Fe_{14}B$ and $a = 5.45$ Å for Nd_4O obtained by our previous study [24]. The crystal structure of Nd_4O is determined by experiments. However, there is no experimental report examining the misorientation angles of Nd_4O against the $Nd_2Fe_{14}B$ main phase at the interface. For the sake of simplicity and reducing the lattice mismatch between the main phase and the subphase, we choose a supercell which is constructed of a $\sqrt{2} \times \sqrt{2} \times 1$ unit cell for $Nd_2Fe_{14}B$ (main phase) and a $\sqrt{5} \times \sqrt{5} \times 2$ unit cell for Nd_4O (subphase). These two structures are aligned with the [001] direction, and the lattice mismatch between these two structures is only 1.2% in the present case. Recent experimental reports on the grain-boundary structure of Nd-Fe-B magnets using scanning transmission electron microscopy show that Nd layers of $Nd_2Fe_{14}B$ appear as the first layer at the interface when grain-boundary phases are parallel to the (001) plane of $Nd_2Fe_{14}B$ grains [25,26]. The subphase is placed on the main phase, and one Cu atom per supercell exists around the interstitial region, as shown in Fig. 1, and our model structures contain more than 200 atoms in a supercell. All the calculations are performed under the assumption that spin configurations in $Nd_2Fe_{14}B$ and Nd_4O are collinear structures for simplicity. Note that the magnetic ground-state structure of $Nd_2Fe_{14}B$ is noncollinear below $T = 135$ K, and the magnetic moments are inclined at $\theta = 30°$ to the [001] direction at $T = 0$ K [1,27]. The magnetic ground state of Nd_4O is unknown in experiments because it is a metastable structure. As reported in experiments [20,21], the total magnetic moment is zero in metallic Nd subphases at room temperature due to thermal fluctuations. This indicates the weak magnetic coupling in Nd_4O at low temperature. In that sense, the magnetic structure of Nd_4O is insignificant. Since both pure Nd and Nd oxides are not ferromagnetic, we assume antiferromagnetic coupling among spin moments of $5d$ electrons in Nd atoms in Nd_4O having the zero magnetic moment. In our model structures, there are five Nd layers in the subphase. The magnetic moment direction of $5d$ electrons in Nd atoms in the first, third, and fifth layers are aligned with [001] and with $[00\bar{1}]$ in the other layers, respectively. We use a $3 \times 3 \times 2k$-point mesh, and a 500-Ry cutoff energy. The convergence criteria for the maximum force on each atom and the total energy are 10^{-3} hartree/bohr and 10^{-6} hartree, respectively.

III. RESULTS AND DISCUSSION

According to experimental reports [11,12], the small amount of Cu atoms is thought to be located around the interface between the main phase and the subphase. We perform DFT calculations for several kinds of grain-boundary model structures shown in Fig. 1, where one Cu atom is located at (i) the interstitial space, which is between the main phase and the subphase $Nd_2Fe_{14}B/Cu/Nd_4O$, and (ii) the Fe site $Nd_2Fe_{14-x}Cu_xB/Nd_4O$. There is no Cu atom in model (iii) $Nd_2Fe_{14}B/Nd_4O$,

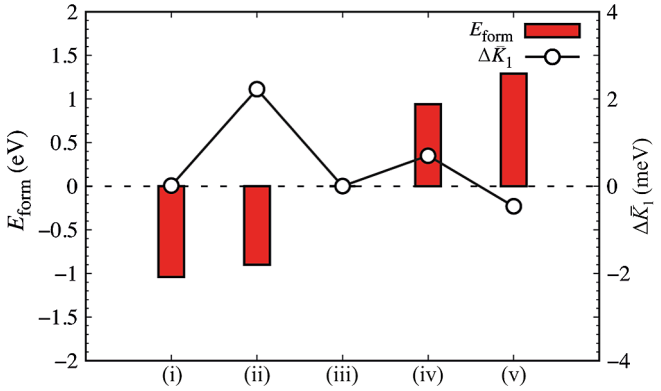

FIG. 2. The bars represent the formation energy E_{form}. The open circles indicate the averaged anisotropy constants $\bar{K}_1$ of Nd at the interface around $z = 12$ Å. $\bar{K}_1$ in model (iii) is set at 0 meV.

and one Cu atom is located at (iv) the Nd site in the main phase $Nd_{2-x}Cu_xFe_{14}B/Nd_4O$ and (v) the Nd site in the subphase $Nd_2Fe_{14}B/Nd_{4-x}Cu_xO$. We define the Cu-defect-formation energy E_{form} as follows:

$$E_{form} = E_{Cu\ doped} - E_{pristine} + \alpha E_{Nd} + \beta E_{Fe} - \gamma E_{Cu}, \quad (1)$$

where $E_{Cu\ doped}$ denotes the total energies of Cu-doped model structures (i), (ii), (iv), and (v), and $E_{pristine}$ represents the total energy of model (iii), which does not contain Cu in the system. The last three energies on the right side of Eq. (1) are the total energies of the double hcp Nd, bcc Fe, and fcc Cu per atom, respectively. Note that α, β, and γ take 0 or 1 depending on the system. The formation energies of these structural-optimized model systems calculated with Eq. (1) are shown in Fig. 2. From the comparison of the formation energies in these model structures, we find that the model structures where the Cu is located at the interstitial space and the Fe site at the interface of the main phase are the most stable among our model structures. Structures with Nd substituted by Cu are not stable because they have higher formation energies than that of model (iii).

The anisotropy of Nd atoms is strongly related to the coercivity and is determined by interactions between $4f$ electrons in Nd atoms and other electrons in surrounding atoms. Hence, in order to analyze the anisotropy of Nd atoms, it is necessary to perform structural optimization in DFT calculations for determining the structures at the interface where potentials around Nd atoms could be distorted. After the calculations of E_{form} for the model systems in which all atomic positions are optimized, we analyze the anisotropy constant K_1 of Nd atoms by calculating the crystal field parameters $A_{20}\langle r^2\rangle$ of Nd atoms which can be evaluated from first-principles calculations [28,29]. Note that we assume the coercivity is related only to the first-order anisotropy term in the anisotropy energy. The anisotropy constant K_1 of Nd is represented as follows;

$$K_1 = -3J(J-1/2)\Theta_{20}A_{20}\langle r^2\rangle, \quad (2)$$

where J is a total angular momentum, Θ_{20} is the Stevens factor, $\langle r^2\rangle$ indicates the average of the radial part of the $4f$ wave function in a Nd atom, and A_{20} is the crystal field coefficient [28,29]. Here, $J = 9/2$ $(L = 6, S = 3/2)$ and $\Theta_{20} = -7/1089$ for Nd^{3+}. The crystal field coefficient can be written

$$A_{20}\langle r^2\rangle = a_{20}\int_0^{r_c} drr^2|R_{4f}(r)|^2V_{20}(r), \quad (3)$$

where $a_{20} = \sqrt{5/16\pi}$, r_c is the cutoff radius, $R_{4f}(r)$ is an atomic radial function of the Nd $4f$, and $V_{20}(r)$ is the effective potential given by solving the Kohn-Sham equation. This approximation is based on the fact that $R_{4f}(r)$ of well-localized Nd $4f$ electrons is insensitive to the surrounding chemical environment. Note that the effective potential $V_{20}(r)$ is affected only by the surrounding environment which determines the direction of the magnetic anisotropy for Nd. In other words, we can evaluate the effects of Cu on the magnetic anisotropy of Nd through $V_{20}(r)$. We calculate the $\bar{K}_1$ difference from model (iii) with Eqs. (2) and (3) shown in Fig. 2. In this figure, we average the anisotropy constant of Nd, $\bar{K}_1$ around 12 Å, because there are three or four Nd atoms at the interface in the main phase where Cu exists. By considering the anisotropy at the interface and the formation energies of our model systems, we can understand the role of Cu that is thought to be able to increase the coercivity in Nd-Fe-B magnets.

As depicted in Fig. 2, models (i) and (ii) are much more stable than model (iii). This suggests that some parts of the interfaces become a structure as model (i) and other parts of them become a structure as model (ii). In other words, the interface structure can be changed from (iii) to (i) and (ii) by the annealing process in the experiments. Model (i) does not show the magnetic anisotropy improvement, in spite of Cu being at the interstitial space. On the other hand, $\bar{K}_1$ in model (ii), which is −3.4 meV plotted in Fig. 3 around 12 Å, improves by 40% compared to that in model (iii), which is −5.7 meV. By considering these results, the total magnetic anisotropy of Nd atoms at the interfaces in a Nd-Fe-B magnet increases since some interfaces have the same structures as model (ii). Therefore, some Cu atoms play important roles of improving the magnetic anisotropy of Nd atoms at the interface by replacing Fe atoms with themselves.

Figure 3 shows the averaged anisotropy constant $\bar{K}_1$ of Nd atoms as a function of the z coordinate in $Nd_2Fe_{14}B$. When $\bar{K}_1 > 0$, the anisotropy of Nd atoms is in the out-of-plane direction. All $\bar{K}_1$'s show a large uniaxial anisotropy at $z = 6$. Most of our model structures show negative $\bar{K}_1$ values at the interfaces on the left and right sides in Fig. 3, which is the same tendency as in previous studies of K_1 of Nd atoms in the surface case [28,29]. From the averaged $\bar{K}_1$

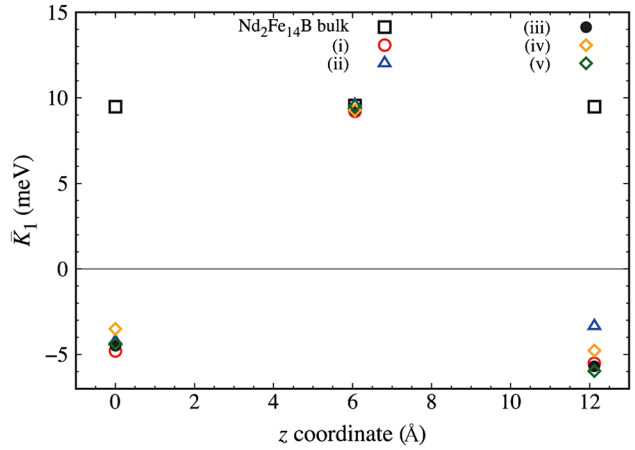

FIG. 3. The averaged anisotropy constants $\bar{K}_1$ of Nd atoms in the $Nd_2Fe_{14}B$ main phase as a function of the z coordinate. In the Cu-doped systems, one Cu atom is located around 12 Å.

at $z = 12.1$ Å, one can see the importance of Cu from the $\bar{K}_1$ improvement in model (ii). In fact, the magnetic anisotropies of four Nd atoms near Cu in model (ii) are −1.7 ($4f$), −8.4 ($4g$), −1.8 ($4g$), and −1.5 ($4f$) meV, respectively, which are improved because of the Cu doping. Here, $4g$ and $4f$ indicate labels of the inequivalent sites for Nd. Note that the magnetic anisotropies of the corresponding Nd atoms in model (iii) are −3.4, −9.0, −8.4, and −5.2 meV, respectively.

In previous studies, the atomic scale Landau-Lifshitz-Gilbert (LLG) equation has been used to study surface effects on the coercivity in Nd-Fe-B magnets [24,30]. These studies have shown that the negative K_1 of rare-earth atoms at the surface triggers the magnetic reversal. This magnetic reversal causes the coercivity decrease due to the domain wall propagating into the internal region of $Nd_2Fe_{14}B$. Combining our result with those of the LLG studies, we conclude that the coercivity improvement in the experiments results from substituting Fe with Cu after the annealing process, which not only decreases the number of Fe atoms at the main-phase interface but also weakens the magnetic coupling between the Nd and Fe atoms. The present DFT study indicates a remarkable improvement of the anisotropy of Nd by means of substituting Fe with Cu at the interface.

Figure 4(a) shows the magnetic moments of Fe atoms in the main phase of the bulk and each model structure. As one can see, the magnetic moments at the interfaces $z = 0$ and 12.1 Å are enhanced compared to that of the bulk system. This is due to the localized electrons in the $d_{x^2-y^2}$ orbital which distributes in the x-y plane.

We calculate the magnetic anisotropy energy (MAE) of Fe atoms in the main phase of the bulk and each model structure shown in Fig. 4(b) with a perturbation scheme [31]. An interesting phenomenon is that the Fe atom located in the same layer as the Nd and B atoms clearly

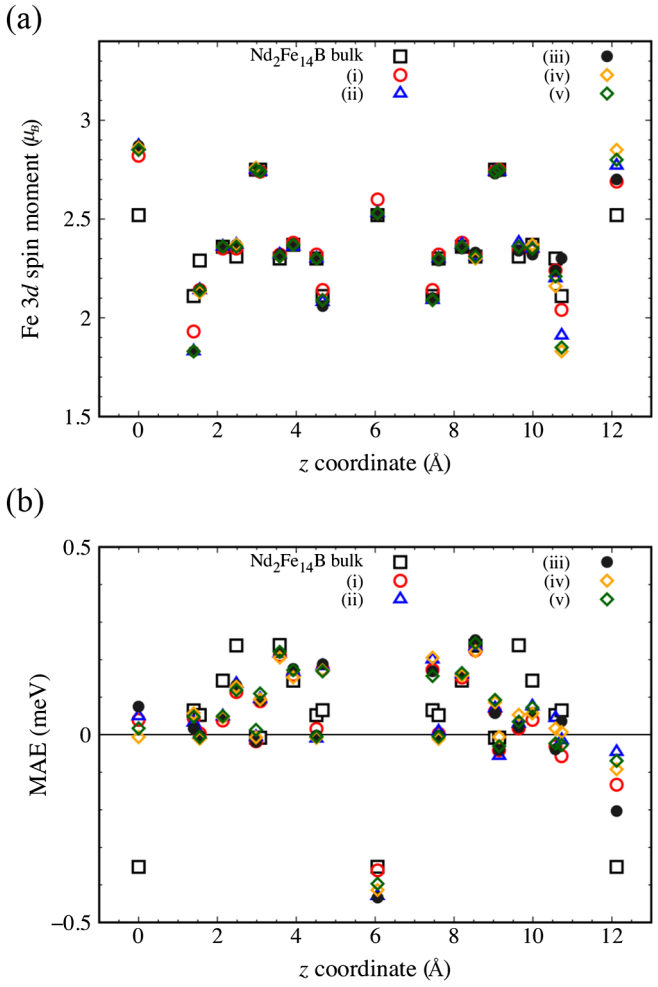

FIG. 4. (a) The averaged magnetic moments of Fe atoms in the $Nd_2Fe_{14}B$ main phase of the bulk and each model structure. (b) The averaged magnetic anisotropy energy of Fe atoms in the $Nd_2Fe_{14}B$ main phase of the bulk and each model structure. Positive and negative MAE indicate the in-plane and out-of-plane anisotropy, respectively. In the Cu-doped systems, one Cu atom is located around 12 Å. Each physical value is plotted as a function of the z coordinate in the bulk system for comparison.

shows remarkable in-plane magnetic anisotropy, in contrast with the out-of-plane anisotropy of most other Fe atoms. The same tendency can be seen in the magnetic anisotropy of Fe in $Y_2Fe_{14}B$, which has the same crystal structure as $Nd_2Fe_{14}B$ [31]. In the same way as the $\bar{K}_1$ at $z = 12.1$ Å in Fig. 3, the MAE of model (ii) improves when Cu substitutes Fe at the main phase interface because of the weak magnetic coupling between Nd and Fe.

As we describe above, we choose the model structures labeled (i) to (v) based on the assumption that Cu might be around the interface. However, we cannot neglect the possibility of Cu atoms being inside the main phase. Thus, we also check the stability of Cu-doped $Nd_2Fe_{14}B$ bulk and surface systems by evaluating the formation energies in order to confirm that Cu atoms should be

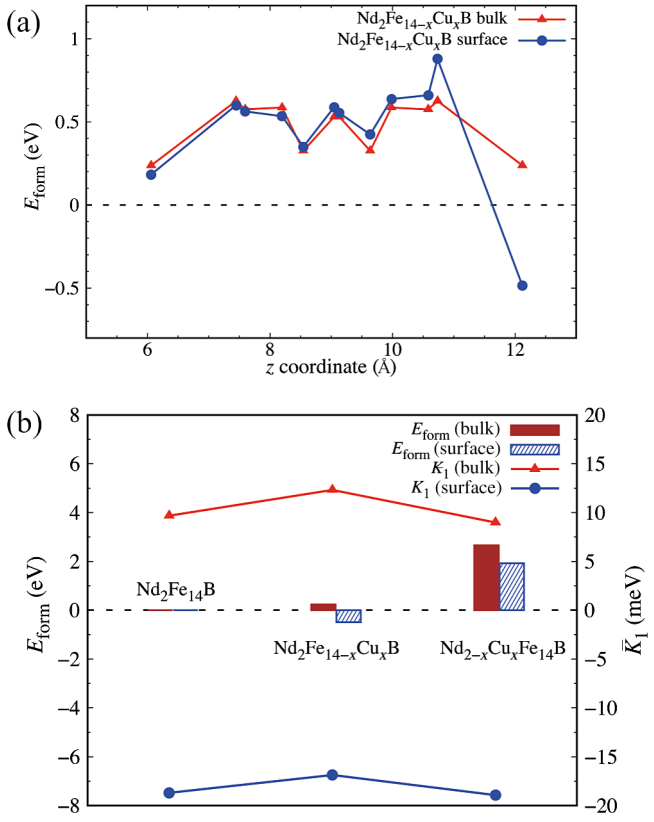

FIG. 5. (a) The formation energy for the pristine bulk or surface system and the one-Fe-atom-substituted systems as a function of the Cu z coordinate. Bulk and surface cases are represented by the closed triangles and circles, respectively. Lines are a guide to the eye. (b) The formation energies of pristine bulk, surface, the one-Fe-atom- and one-Nd-atom-substituted $Nd_2Fe_{14}B$ systems with Cu at $z = 12.1$ Å and those of the averaged anisotropies in Nd at the same layer of Cu. The averaged anisotropies $\bar{K}_1$ of Nd atoms, which are at the same layer as the Cu, are plotted with lines for the bulk and surface systems. In both figures, the total energies of the pristine bulk and surface systems are set at 0 eV represented by the horizontal dotted line.

around the interface. The surface is at $z = 12.1$ Å, and the vacuum is from $z = 12.1$ to 22.1 Å. Figure 5(a) shows the formation energy of Fe-substituted $Nd_2Fe_{14}B$ bulk and surface systems with one Cu atom per supercell as a function of the Cu z coordinate in $Nd_2Fe_{14}B$. We discover that the Fe-substituted systems with Cu that is located in the same layer of the Nd and B atoms existing around $z = 6$ and 12.1 Å, generally have lower formation energy than other Fe-substituted systems in the bulk and the surface cases. Especially in the surface model, Fe atoms at the surface can be replaced easily by Cu atoms because the formation energy is lower than at other Fe sites. These lower formation energies at $z = 6$ and 12.1 Å can be related to the negative MAE around $z = 0$, 6, and 12.1 Å in Fig. 4(b) for the $Nd_2Fe_{14}B$ bulk system. As an illustration, the formation energies of Nd-substituted $Nd_2Fe_{14}B$ bulk and surface systems with one Cu atom at $z = 12.1$ Å are given in Fig. 5(b). One can see that substituting Nd with Cu is unstable in the bulk and the surface systems. In addition, the $\bar{K}_1$ improvement can be seen also in the Fe-substituted surface and bulk systems illustrated in Fig. 5(b). This situation is similar to the case of model (ii), as we explain above. Hence, these analyses support our choice of the grain-boundary model structures (i) to (v) where Cu atoms do not exist in the inner region of the main phase but do exist around the interstitial region.

IV. CONCLUSIONS

In conclusion, we use first-principles calculations to understand the mechanism of the coercivity improvement in Nd-Fe-B magnets by Cu. We find that the anisotropies of Fe and Nd atoms at the interface are essentially negative. Considering the negative anisotropy of these atoms and the formation energy analysis, we conclude that substituting the Fe site with Cu at the main-phase interface can be realized in the annealing process. This works effectively in terms of improving the coercivity since the anisotropy of Nd improves by 40% compared with the non-Cu-doped system, thanks to substituting Cu for the Fe atom that has negative anisotropy. Introducing Cu around the interface between main-phase grains and subphases prevents domain walls from penetrating into main-phase grains. This Cu addition around the interface can cause the coercivity enhancement after the Nd-Cu grain-boundary diffusion process. We hope this investigation will be helpful for experimental processes of making high-performance Nd-Fe-B magnets by controlling Cu around the interface.

ACKNOWLEDGMENTS

Part of this work is supported by the Elements Strategy Initiative Project under the auspice of MEXT. We are grateful to Dr. S. Hirosawa, Dr. K. Hono, Dr. T. Ohkubo, and Professor T. Ozaki for fruitful discussions. This research result is partly carried out by using computational resources of the K computer (Grants No. hp120086, No. hp140150, No. hp140214, No. hp150014, and No. cmsi0205) and supercomputers at ISSP and ITC, The University of Tokyo.

[1] J. M. D. Coey, *Magnetism and Magnetic Materials* (Cambridge University Press, Cambridge, England, 2010).
[2] J. F. Herbst, $R_2Fe_{14}B$ materials: Intrinsic properties and technological aspects, Rev. Mod. Phys. **63**, 819 (1991).
[3] J. M. D. Coey, Permanent magnets: Plugging the gap, Scr. Mater. **67**, 524 (2012).
[4] J. J. Croat, J. F. Herbst, R. W. Lee, and F. E. Pinkerton, PrFe- and NdFe-based materials: A new class of high performance permanent magnets (invited), J. Appl. Phys. **55**, 2078 (1984).

[5] M. Sagawa, S. Fujimura, N. Togawa, H. Yamamoto, and Y. Matsuura, New material for permanent magnets on a base of Nd and Fe (invited), J. Appl. Phys. **55**, 2083 (1984).
[6] M. Sagawa, S. Fujimura, H. Yamamoto, Y. Matsuura, and S. Hirosawa, Magnetic properties of rare-earth iron boron permanent magnet materials, J. Appl. Phys. **57**, 4094 (1985).
[7] T. Schrefl, J. Fidler, and H. Kronmüller, Remanence and coercivity in isotropic nanocrystalline permanent magnets, Phys. Rev. B **49**, 6100 (1994).
[8] S. Hirosawa, Current status of research and development toward permanent magnets free from critical elements, J. Magn. Soc. Jpn. **39**, 85 (2015).
[9] J. Fidler and J. Bernardi, Transmission electron microscope characterization of cast and hotworked RFeB : Cu (R = Nd, Pr) permanent magnets, J. Appl. Phys. **70**, 6456 (1991).
[10] M. Takezawa, Y. Nagashima, Y. Kimura, Y. Morimoto, J. Yamasaki, N. Nozawa, T. Nishiuchi, and S. Hirosawa, Magnetic domain observation of Nd-Cu-diffused Nd-Fe-B magnets with submicron grains by Kerr effect microscopy, J. Appl. Phys. **111**, 07A714 (2012).
[11] H. Sepehri-Amin, T. Ohkubo, T. Shima, and K. Hono, Grain boundary and interface chemistry of an Nd-Fe-B-based sintered magnet, Acta Mater. **60**, 819 (2012).
[12] H. Sepehri-Amin, T. Ohkubo, S. Nagashima, M. Yano, T. Shoji, A. Kato, T. Schrefl, and K. Hono, High-coercivity ultrafine-grained anisotropic Nd-Fe-B magnets processed by hot deformation and the Nd-Cu grain boundary diffusion process, Acta Mater. **61**, 6622 (2013).
[13] A. Kianvash and I. R. Harris, Magnetic properties of the sintered magnets produced from a NdFeBCu-type material, J. Appl. Phys. **70**, 6453 (1991).
[14] J. Bernardi and J. Fidler, Preparation and transmission electron microscope investigation of sintered $Nd_{15.4}Fe_{75.7}B_{6.7}Cu_{1.3}Nb_{0.9}$ magnets, J. Appl. Phys. **76**, 6241 (1994).
[15] M. Velicescu, W. Fernengel, W. Rodewald, P. Schrey, and B. Wall, High-energy sintered NdDyFeB magnets with Co and Cu additions, J. Magn. Magn. Mater. **157–158**, 47 (1996).
[16] F. Vial, F. Joly, E. Nevalainen, M. Sagawa, K. Hiraga, and K. T. Park, Improvement of coercivity of sintered NdFeB permanent magnets by heat treatment, J. Magn. Magn. Mater. **242–245**, 1329 (2002).
[17] S. Pandian, V. Chandrasekaran, G. Markandeyulu, K. J. L. Iyer, and K. V. S. R. Rao, Effect of Al, Cu, Ga, and Nb additions on the magnetic properties and microstructural features of sintered NdFeB, J. Appl. Phys. **92**, 6082 (2002).
[18] H. J. Engelmann, A. S. Kim, and G. Thomas, Microstructure and magnetic effects of small Cu additions to (Nd,Dy)FeB magnets, Scr. Mater. **36**, 55 (1997).
[19] A. Yasui, T. Nakamura, Y. Kotani, T. Fukagawa, T. Nishiuchi, and S. Hirosawa, Temperature dependence of post-sintered annealing on magnetic properties of intergranular phase in Nd-Fe-B permanent magnet, J. Appl. Phys. **117**, 17B313 (2015).
[20] T. Fukagawa and S. Hirosawa, Coercivity generation of surface $Nd_2Fe_{14}B$ grains and mechanism of fcc-phase formation at the $Nd/Nd_2fe_{14}B$ interface in Nd-sputtered Nd-Fe-B sintered magnets, J. Appl. Phys. **104**, 013911 (2008).
[21] T. Fukagawa, S. Hirosawa, T. Ohkubo, and K. Hono, The effect of oxygen on the surface coercivity of Nd-coated Nd-Fe-B sintered magnets, J. Appl. Phys. **105**, 07A724 (2009).
[22] T. Ozaki, Variationally optimized atomic orbitals for large-scale electronic structures, Phys. Rev. B **67**, 155108 (2003).
[23] J. P. Perdew, K. Burke, and M. Ernzerhof, Generalized Gradient Approximation Made Simple, Phys. Rev. Lett. **77**, 3865 (1996).
[24] H. Misawa, Ph.D. thesis, The University of Tokyo, 2015.
[25] T. T. Sasaki, T. Ohkubo, and K. Hono, Structure and chemical compositions of the grain boundary phase in Nd-Fe-B sintered magnets, Acta Mater. **115**, 269 (2016).
[26] T. T. Sasaki, T. Ohkubo, Y. Une, H. Kubo, M. Sagawa, and K. Hono, Effect of carbon on the coercivity and microstructure in fine-grained Nd-Fe-B sintered magnet, Acta Mater. **84**, 506 (2015).
[27] D. Givord, H. S. Li, and R. Perrier de la Bâthie, Magnetic properties of $Y_2Fe_{14}B$ and $Nd_2Fe_{14}B$ single crystals, Solid State Commun. **51**, 857 (1984).
[28] H. Moriya, H. Tsuchiura, and A. Sakuma, First principles calculation of crystal field parameter near surfaces of $Nd_2Fe_{14}B$, J. Appl. Phys. **105**, 07A740 (2009).
[29] S. Tanaka, H. Moriya, H. Tsuchiura, A. Sakuma, M. Diviš, and P. Novák, First principles study on the local magnetic anisotropy near surfaces of $Dy_2Fe_{14}B$ and $Nd_2Fe_{14}B$ magnets, J. Appl. Phys. **109**, 07A702 (2011).
[30] C. Mitsumata, H. Tsuchiura, and A. Sakuma, Model calculation of magnetization reversal process of hard magnet in $Nd_2Fe_{14}B$ system, Appl. Phys. Express **4**, 113002 (2011).
[31] Z. Torbatian, T. Ozaki, S. Tsuneyuki, and Y. Gohda, Strain effects on the magnetic anisotropy of $Y_2Fe_{14}B$ examined by first-principles calculations, Appl. Phys. Lett. **104**, 242403 (2014).